

A fault monitoring method for wind power generation system based on sliding mode observer

WENXIN YU^{1,2} , SHAO DAO HUANG¹, DAN JIANG²

¹College of Electrical and Information Engineering, Hunan University
Hunan Province, Changsha, 410082, China

²School of Information and Electrical Engineering
Hunan University of Science and Technology
Hunan Province, Xiangtan, 411201, China
e-mail: slowbird@sohu.com

(Received: 23.12.2019, revised: 01.04.2020)

Abstract: In this paper, a rotor current fault monitoring method is proposed based on a sliding mode observer. Firstly, the state-space model of the Double-Fed Induction Generator (DFIG) is constructed by vector transformation. Meanwhile, the stator voltage orientation vector control method is applied to decouple a stator and rotor currents, so as to obtain the correlation between the stator and rotor current. Furthermore, the mathematical model of stator voltage orientation is obtained. Then a state sliding mode observer (SMO) is established for the output current of the rotor of the DFIG. The stability and reachability of the system in a limited time is proved. Finally, the system state is determined by the residuals of the measured and estimated rotor currents. The simulation results show that the method proposed in this paper can effectively monitor the status: a normal state, voltage drop faults, short-circuit faults between windings, and rotor current sensor faults which have the advantages of fast response, high stability.

Key words: double-fed induction generator (DFIG), sliding model observer (SMO), stator voltage-oriented

1. Introduction

Wind power systems are often installed in remote, inaccessible or unpopular areas where humans have long-term stays. For a long time, planned maintenance and after-the-fact maintenance have been used. A planned safeguard is routine maintenance after 2 500 h or 5 000 h of operation, and it is impossible to understand the condition of the equipment fully and timely; after-sales maintenance is a long-term work, and the loss is significant. Studies have shown that if effective equipment fault detection and diagnostics can be taken, which can continuously monitor different



parameters in the operation of the wind turbine, it is possible to obtain various information reflecting the operation status of wind turbines in real time. After various information is analyzed and processed, the status report and diagnosis results of the equipment operation will be given, and maintenance and overhaul may be arranged. An equipment accident rate can be reduced by 75% roughly, maintenance costs by 25%–50%, and a profitable investment ratio of 17:1 can be obtained. While the safety of the wind turbine is improved greatly, the cost of wind power generation can be reduced effectively. Therefore, the research that significantly reduces maintenance costs and improves the economics of wind turbine operation is very important.

Due to the relatively weak anti-disturbance power of the small capacity converter of a DFIG, the power grid fault has a great influence on the DFIG. When the grid has a major fault, the network voltage drops and the line current increases sharply, which causes the DFIG rotor current to rise and the DC bus voltage to rise. Meanwhile, it leads to the threat on the safety of power electronics. Reference [1] proposes the application of long short term memory network for fault diagnosis in the DFIG system, which is used to detect the faults of open circuit switches of back-to-back converters. Reference [2] introduces detailed theoretical and experimental studies of the DFIG during voltage dips. The behavior characteristics of rotor voltage during voltage sag are well explained in this paper. However, the effect on the rotor current controller is not described. In [3–4], the fault characteristics of the DFIG in different types of power grid faults are analyzed from the theoretical and simulation aspects, and the short circuit currents suitable for various fault conditions are derived. The ability of the doubly-fed wind power generation system to operate uninterruptedly under the condition of grid voltage drop failure is improved. In [5], a low voltage ride through a control method for doubly-fed wind turbines based on passive theory is proposed. In [6], the controllability of the DFIG under unbalanced voltage drop is analyzed, and the critical value of stator voltage and the controllable condition of a rotor side converter are given after voltage drop.

The DFIG has a bad operating environment, complex operating conditions, and a high failure rate. The failure of stator windings and rotor windings is one of the main causes of induction motor failure. In [7], the winding function model of the DFIG is utilized to simulate the stator turn-to-turn fault, and the generation mechanism of the rotor specific harmonic component as well as the stator turn-to-turn fault monitoring method are discussed in depth. In [8], an online detection and diagnosis method for stator winding faults of doubly fed wind turbines by rotor instantaneous power spectrum analysis is proposed. This method is more sensitive than traditional voltage spectrum and current spectrum methods. In [9], the DFIG hybrid (ABC and $d, q, 0$ coordinate system) model of the stator turn-to-turn fault is established. By simulating and analyzing the fault, a detection method based on stator current signal wavelet analysis is proposed. In [10], a diagnosis method based on current estimation difference as a fault characteristic is proposed for the short circuit fault between turns of stator windings of a DFIG.

As the basic component of the wind power generation system, the sensor transmits the most comprehensive data to the data collection system, and the data acquisition system transmits the data to the main control system. After analysis and processing, the control command is issued. There are many kinds of sensors. The installation position is special, and the fault occurs frequently. In particular, if a fault occurs from the sensor, but its output signal is used as the input of the system controller, the closed-loop feedback control will be affected. Thus, the abnormal control amount of the wind power system is output, which results in the system performance degradation.

However, it is difficult for traditional manual maintenance to find the fault in time. Therefore, real-time fault diagnosis of sensor units in wind power generation system has become an urgent research topic. In [11], in order to detect the fault of the load sensor at the root of the wind turbine blade, the dynamic characteristic model of the blade was established and the kalman filter was designed. The fault diagnosis of the sensor is implemented by analyzing the residual between the predicted value of the filter and the sensor measurement. [12] designed a robust observer for fault detection and isolation of sensors in the wind power generation system, which overcame the external interference and uncertainty and improved the system stability, but the overall situation and real-time performance of the system are poor. In [13], for the wind power generation system based on the DFIG, a T-S model is adopted to deal with the nonlinearity in sensor fault diagnosis, and “virtual dynamics” of output error is introduced to avoid complex LMI decoupling and conversion problems. However, the stability of the system cannot be guaranteed reliably. In [14], the approach of sensor fault diagnosis based on an SMO for the nonlinear wind turbine system (WTS) is proposed. In [15], a filter method for fault detection and isolation strategies is proposed for the transducer fault variable speed wind energy conversion system. In [16], an adaptive stator current observer is proposed based on the model reference adaptive method, which implements the fault-tolerant control of the stator current sensor after fault diagnosis.

At present, the common fault monitoring methods of the wind power generation system can be classified into three categories: a model method, signal processing method and artificial intelligence method. The model approach utilizes a deep understanding of the internal structure of the system and requires an accurate mathematical model of the diagnosed object. Model-based methods can be divided into an observer method, equivalent space method and parameter estimation method. By establishing the mathematical model of a DFIG, some scholars employ the observer method to detect the fault of a wind turbine, which is currently the most widely used method for fault detection and diagnosis.

Inspired by [19–22], a method of rotor current fault monitoring for a DFIG is proposed based on sliding mode observer in this paper. The fault monitoring of the wind power generation system under different wind speeds is realized by comparing the residual value of rotor current with the observed value. The paper is structured as follows: in the second part, the stator flux-oriented vector control method is used to construct the mathematical model of the DFIG. An SMO is designed based on the equation model of the DFIG, and the stability is analyzed in the third part. Finally, this paper mainly sets four different types of state of the DFIG: a normal state, voltage drop fault, short-circuit fault between turns of winding and rotor current sensor fault. System faults under different conditions are detected and analyzed by building a Simulink simulation model. The results show that the sliding mode observer designed in this paper can track the rotor current well, and has good performance such as fast response and good stability and so on.

2. Establishment of mathematical model of DFIG

In the paper, the studied DFIG is a wound rotor three-phase asynchronous motor. When all reference variables and parameters are specified, the d, q -axis equivalent circuit of the DFIG can be established. The dynamic DFIG models consists of voltage, flux, and motion equations in a d, q synchronous reference frame are expressed as follows [17–18]:

Voltage equation:

$$\begin{cases} u_{ds} = R_s i_{ds} + \frac{d\psi_{ds}}{dt} - \omega_s \psi_{qs} \\ u_{qs} = R_s i_{qs} + \frac{d\psi_{qs}}{dt} - \omega_s \psi_{ds} \end{cases}, \quad (1)$$

$$\begin{cases} u_{dr} = R_r i_{dr} + \frac{d\psi_{dr}}{dt} - \omega_f \psi_{qr} \\ u_{qr} = R_r i_{qr} + \frac{d\psi_{qr}}{dt} - f \psi_{dr} \end{cases}. \quad (2)$$

Flux equation:

$$\begin{cases} \psi_{ds} = L_s i_{ds} + L_m i_{dr} \\ \psi_{qs} = L_s i_{qs} + L_m i_{qr} \end{cases}, \quad (3)$$

$$\begin{cases} \psi_{dr} = L_m i_{ds} + L_r i_{dr} \\ \psi_{qr} = L_m i_{qs} + L_r i_{qr} \end{cases} \quad (4)$$

and

$$\begin{cases} L_s = L_{\sigma s} + L_m \\ L_r = L_{\sigma r} + L_m \end{cases},$$

where: $u_{ds}, u_{qs}, u_{dr}, u_{qr}$ are the voltage vectors of the stator and rotor of the d, q -axes, respectively; the flux $i_{ds}, i_{qs}, i_{dr}, i_{qr}$ are the current vectors of the stator and rotor of the d, q -axes; $\psi_{ds}, \psi_{qs}, \psi_{dr}, \psi_{qr}$ are t vectors of the stator and rotor of the d, q -axes; R_s, R_r are the rotor and stator resistance; L_s, L_r are the self-inductance of the stator and the rotor; L_m is the mutual inductance between the stator and the rotor; $L_{\sigma s}, L_{\sigma r}$ are the leakage inductance of the stator and rotor; and $\omega_r, \omega_s, \omega_f$ are the rotor speed, synchronous speed and slip speed, respectively. When the d, q current component is used as the state variable and the d, q voltage component is used as the input, the state equation of the DFIG is as follows:

$$\begin{bmatrix} i_{ds} \\ i_{qs} \\ i_{dr} \\ i_{qr} \end{bmatrix} = \frac{1}{\sigma} \begin{bmatrix} \frac{-R_s}{L_s} & \omega_s - \frac{\omega_f L_m^2}{L_s L_r} & \frac{R_r L_m}{L_s L_r} & \frac{\omega_s - \omega_f}{L_s} L_m \\ \frac{\omega_f L_m^2}{L_s L_r} - \omega_s & \frac{-R_s}{L_s} & \frac{\omega_f - \omega_s}{L_s} L_m & \frac{R_r L_m}{L_s L_r} \\ \frac{R_r L_m}{L_s L_r} & \frac{\omega_f - \omega_s}{L_s} L_m & \frac{-R_s}{L_s} & \omega_f - \frac{\omega_s L_m^2}{L_s L_r} \\ \frac{\omega_s - \omega_f}{L_s} L_m & \frac{R_r L_m}{L_s L_r} & \frac{\omega_s L_m^2}{L_s L_r} - \omega_f & \frac{-R_s}{L_s} \end{bmatrix} \begin{bmatrix} i_{ds} \\ i_{qs} \\ i_{dr} \\ i_{qr} \end{bmatrix} + \begin{bmatrix} \frac{1}{\sigma L_s} & 0 & \frac{L_m}{\sigma L_s L_r} & 0 \\ 0 & \frac{1}{\sigma L_s} & 0 & -\frac{L_m}{\sigma L_s L_r} \\ -\frac{L_m}{\sigma L_s L_r} & 0 & \frac{1}{\sigma L_s} & 0 \\ 0 & -\frac{L_m}{\sigma L_s L_r} & 0 & \frac{1}{\sigma L_s} \end{bmatrix}, \quad (5)$$

where

$$\sigma = 1 - \frac{L_m^2}{L_s L_r}.$$

Only the rotor current term is considered in this paper, whose state space model is as follows.

$$\begin{cases} \dot{i}_r = A_0 i_r + A_1 i_s + B_u \\ y = C i_r \end{cases}, \quad (6)$$

where: $i_r = [i_{dr} \ i_{qr}]$ is set as the state variable of the system, $i_s = [i_{ds} \ i_{qs}]$ and $u = [u_{ds}, u_{qs}, u_{dr}, u_{qr}]$ are set as the inputs of the system. y is set as the output vector of the system, and C is set as the output matrix of the system, where:

$$A_0 = \frac{1}{\sigma} \times \begin{bmatrix} \frac{-R_s}{L_s} & \omega_f - \frac{\omega_s L_m^2}{L_s L_r} \\ \frac{\omega_s L_m^2}{L_s L_r} - \omega_f & \frac{-R_s}{L_s} \end{bmatrix}, \quad A_1 = \begin{bmatrix} \frac{R_s L_m}{\sigma L_s L_r} & \frac{\omega_f - \omega_s}{\sigma L_r} L_m \\ \frac{\omega_s - \omega_f}{\sigma L_r} L_m & \frac{R_s L_m}{\sigma L_s L_r} \end{bmatrix},$$

$$B = \begin{bmatrix} \frac{-L_m}{\sigma L_s L_r} & 0 & \frac{1}{\sigma L_r} & 0 \\ 0 & \frac{-L_m}{\sigma L_s L_r} & 0 & \frac{1}{\sigma L_s} \end{bmatrix}, \quad C = \begin{bmatrix} 1 & 0 \\ 0 & 1 \end{bmatrix}.$$

Since the circuit of the variable-speed constant-frequency DFIG has magnetic coupling, vector control is adopted in this paper to achieve decoupling of active power and reactive power. The three-phase current of the stator in the three-phase stationary coordinate system is subjected to d, q rotation coordinate transformation. It is decomposed into the excitation current component and the torque current component. It is similar to the torque control of a DC motor.

The excitation current component remains unchanged during the speed regulation process. Its speed regulation can be achieved by electromagnetic torque, which can be controlled by the torque current component. Voltage oriented vector control technology is adopted in this paper.

The stator voltage space vector of the DFIG is oriented on the d -axis under the synchronous rotation d, q coordinate. Then the stator voltage, a component of the d, q -axes, can be expressed as (7).

However, in practical applications, the reactance is larger than the resistance with increasing power, especially for high-power DFIGs. Therefore, the voltage drop across the stator resistance is much smaller than the total voltage drops. The direct consequence is that the angle between the stator voltage and the flux linkage is approximately 90° . The stator resistance is ignored in this paper. Therefore, there is no difference between the stator flux linkage orientation and the stator voltage orientation. Then, its stator flux linkage can be expressed as (8). And Equation (9) can be obtained by bringing Equations (7) and (8) into Equations (1) and (3).

$$\begin{cases} u_{qs} = 0 \\ u_{ds} = -\omega_s \psi_s \end{cases}, \quad (7)$$

$$\begin{cases} \psi_{ds} = 0 \\ \psi_{qs} = \psi_s \end{cases}, \quad (8)$$

$$\begin{cases} i_{ds} = \frac{-L_m i_{dr}}{L_s} \\ i_{qs} = \frac{\psi_s - L_m i_{qr}}{L_s} \end{cases}, \quad (9)$$

where ψ_s is the amplitude of stator flux. Equation (10) can be calculated by putting Equation (9) into the rotor current state space model (6), where the stator current term is replaced by the rotor current term.

$$\begin{cases} \begin{bmatrix} \dot{i}_{dr} \\ \dot{i}_{qr} \end{bmatrix} = A_0 \begin{bmatrix} i_{dr} \\ i_{qr} \end{bmatrix} + A_1 \begin{bmatrix} \frac{-L_m i_{dr}}{L_s} \\ \frac{\psi_s - L_m i_{qr}}{L_s} \end{bmatrix} + Bu \\ y = Ci_r \end{cases}. \quad (10)$$

3. Design of sliding mode observer(SMO) for DFIG

In the actual DFIG system, not all state variables can be measured. But the inputs and outputs of the system can be measured. Thus, a SMO is designed based on the rotor current to the DFIG system. Next, the fault of the DFIG system can be diagnosed. The SMO is designed as follows. First, Equation (10) is simplified to Equation (11):

$$\begin{cases} \dot{i}_r = Ai_r + Bu + f \\ u = Ci_r \end{cases}, \quad (11)$$

where:

$$A = \begin{bmatrix} -\frac{R_s L_m^2}{\sigma L_s^2 L_r} - \frac{R_r}{\sigma L_r} & \omega_f \\ -\omega_f & -\frac{R_s L_m^2}{\sigma L_s^2 L_r} - \frac{R_r}{\sigma L_r} \end{bmatrix}, \quad B = \begin{bmatrix} \frac{-L_m}{\sigma L_s L_r} & 0 & \frac{1}{\sigma L_r} & 0 \\ 0 & \frac{-L_m}{\sigma L_s L_r} & 0 & \frac{1}{\sigma L_s} \end{bmatrix},$$

$$f = \begin{bmatrix} \frac{\omega_f - \omega_s}{\sigma L_r L_s} L_m \psi_s \\ \frac{R_s L_m \psi_s}{\sigma L_s^2 L_r} \end{bmatrix}.$$

According to Formula (11) and sliding mode variable structure control theory, the structure of the sliding mode observer is constructed as follows:

$$\begin{cases} \dot{\tilde{i}}_r = A\tilde{i}_r + Bu + f + \tilde{v} \\ u = C\tilde{i}_r \end{cases}, \quad (12)$$

where: $\tilde{i}_r = [\tilde{i}_{dr} \ \tilde{i}_{qr}]^T$ is the estimated value of the rotor current, \tilde{v} is the control rate of the sliding mode observer, and $\tilde{v} = [v \ g \times v]^T$, where g is the parameter.

The given error amount e is shown in (13) below.

$$e = \begin{bmatrix} e_1 \\ e_2 \end{bmatrix} = \begin{bmatrix} i_{dr} - \tilde{i}_{dr} \\ i_{qr} - \tilde{i}_{qr} \end{bmatrix}. \quad (13)$$

$s = c \times e_1 + e_2 = 0$ is chosen as the sliding mode surface (switching function), where c is the parameter.

Equation (14) can be obtained according to Equations (11) and (12).

$$\begin{aligned} \dot{s} &= c \times \dot{e}_1 + \dot{e}_2 = \\ &= \left(c \times \left(-\frac{R_s L_m^2}{q L_s^2 L_r} - \frac{R_r}{q L_r} \right) - \omega_f \right) e_1 + \left(-\frac{R_s L_m^2}{q L_s^2 L_r} - \frac{R_r}{q L_r} + c \times \omega_f \right) e_2 - (g + c) \times v. \end{aligned} \quad (14)$$

The value v can be calculated.

$$v = \left(\frac{1}{g + c} \right) \times \left(\left(c \times \left(-\frac{R_s L_m^2}{q L_s^2 L_r} - \frac{R_r}{q L_r} \right) - \omega_f \right) e_1 + \left(-\frac{R_s L_m^2}{q L_s^2 L_r} - \frac{R_r}{q L_r} + c \times \omega_f \right) e_2 - s \right).$$

The approach rate \dot{s} is set to $\dot{s} = -ks - \varepsilon \operatorname{sgn}(s)$.

Then

$$\begin{aligned} v &= \left(\frac{1}{g + c} \right) \times \left(\left(c \times \left(-\frac{R_s L_m^2}{q L_s^2 L_r} - \frac{R_r}{q L_r} \right) - \omega_f \right) e_1 + \right. \\ &\quad \left. + \left(-\frac{R_s L_m^2}{q L_s^2 L_r} - \frac{R_r}{q L_r} + c \times \omega_f \right) e_2 + ks - \varepsilon \operatorname{sgn}(s) \right). \end{aligned} \quad (15)$$

Theorem 1: For the sliding mode variable structure control system, based on the selection of its switching function, its Lyapunov function is defined as Equation (16).

$$V = \frac{1}{2} s^2. \quad (16)$$

If $k > 0$, $\varepsilon > 0$ is satisfied,

$$\dot{V} = s \times \dot{s} \leq 0.$$

Then the control system is gradually stable.

Proof:

$$\begin{aligned} s \cdot \dot{s} &= s \cdot \left[\left(c \cdot \left(-\frac{R_s L_m^2}{\sigma L_s^2 L_r} - \frac{R_r}{\sigma L_r} \right) - \omega_f \right) e_1 + \left(-\frac{R_s L_m^2}{\sigma L_s^2 L_r} - \frac{R_r}{\sigma L_r} + c \cdot \omega_f \right) e_2 - (g + c) \cdot v \right] \\ &= s \cdot \left[\left(c \cdot \left(-\frac{R_s L_m^2}{\sigma L_s^2 L_r} - \frac{R_r}{\sigma L_r} \right) - \omega_f \right) e_1 + \left(-\frac{R_s L_m^2}{\sigma L_s^2 L_r} - \frac{R_r}{\sigma L_r} + c \cdot \omega_f \right) e_2 - (g + c) \cdot \left(\frac{1}{g + c} \right) \right. \\ &\quad \left. \cdot \left(\left(c \cdot \left(-\frac{R_s L_m^2}{\sigma L_s^2 L_r} - \frac{R_r}{\sigma L_r} \right) - \omega_f \right) e_1 + \left(-\frac{R_s L_m^2}{\sigma L_s^2 L_r} - \frac{R_r}{\sigma L_r} + c \cdot \omega_f \right) e_2 + ks + \varepsilon \operatorname{sgn}(s) \right) \right] \\ &= s \cdot (-ks - \varepsilon \operatorname{sgn}(s)) = -ks^2 - \varepsilon \operatorname{sgn}(s) \cdot s. \end{aligned}$$

When $k > 0$, $\varepsilon > 0$, then $\dot{V} \leq 0$, so the stability of the control system can be proved.

Inspired by [23], theorem 2 is obtained, and the theorem mainly shows that the reach time is limited.

Theorem 2: If the approach law $\dot{s} = -ks - \varepsilon \text{sgn}(s)$ can be satisfied, the system reaches the sliding surface $s(t) = 0$ within the finite time T , where:

$$T \leq \frac{1}{k} \ln \left(1 + \frac{k}{\varepsilon} \|s(0)\| \right).$$

Proof:

$$s^T \dot{s} = \frac{1}{2} \frac{ds^2}{dt} = \frac{1}{2} \frac{d|s|^2}{dt} = |s| \frac{d|s|}{dt},$$

$$s^T \text{sgn } s = \|s\|_1 \leq \|s\|.$$

Thereby

$$\frac{d\|s\|}{dt} < -k\|s\| - \varepsilon. \tag{17}$$

Formula (18) can be derived by the integral from 0 to t of Formula (17).

$$\frac{\varepsilon}{k} (e^{kT} - 1) \leq \|s(0)\|. \tag{18}$$

Formula (19) can finally be calculated.

$$T \leq \frac{1}{k} \ln \left(1 + \frac{k}{\varepsilon} \|s(0)\| \right). \tag{19}$$

The DFIG control structure diagram of the stator flux linkage based on the sliding mode observer is shown in Fig. 1. When the doubly-fed induction generator works normally, the observer rotor current measurement value does not deviate from the estimated value. However, when a fault occurs, the residual error is not zero.

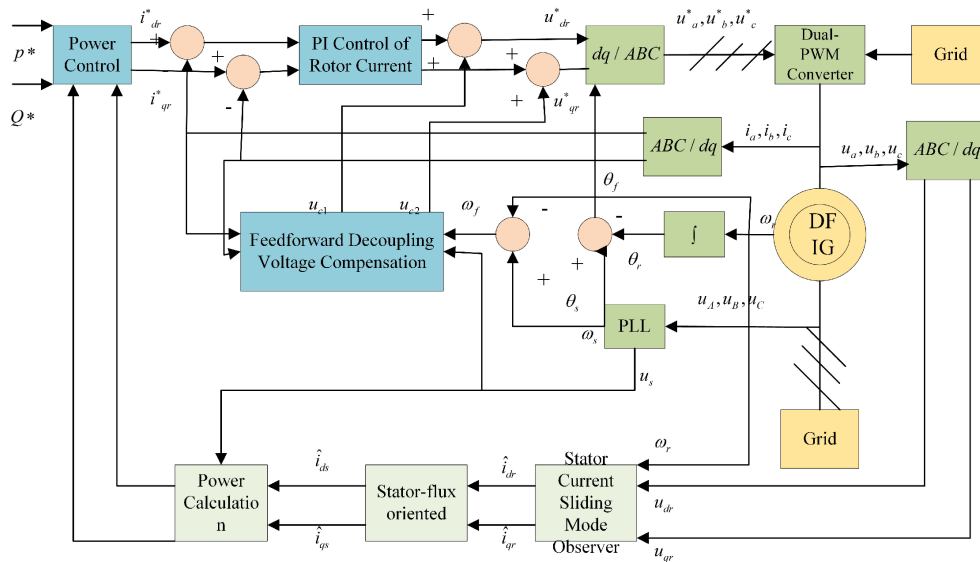


Fig. 1. DFIG control structure diagram of stator flux linkage based on sliding mode observer

4. Fault design and simulation analysis

In this paper, four conditions (no fault, power grid terminal voltage drop fault, DFIG winding fault and rotor current sensor fault) are considered. In order to verify the feasibility and correctness of the proposed method, the DFIG simulation model of vector control is built by MATLAB/SIMULINK. Furthermore, the fault monitoring of the system can be realized by observing the residual value between the observed rotor current output by the sliding mode observer and the actual value. In addition, the main parameters of this paper are set as follows.

Table 1. Main parameters of the DFIG system

Item	Value	Item	Value
Grid voltage (V)	220	Nominal power (VA)	3 730
Grid frequency (Hz)	50	Voltage (line–line) (V)	460
DC bus voltage	600	Pole pairs	4
Wind speed (m/s)	< 12	R_s (Ω)	1.115
Blade radius of wind turbine (m)	2	R_r (Ω)	1.083
Gear box transmission ratio	1 : 3	$L_{\sigma s}, L_{\sigma r}$ (mH)	5.974
		L_m (H)	0.2037

1. No fault

In the case of no fault, $c = 2$, $g = 0.1$, $k = 5\,000$, $\varepsilon = 3\,000$ are set as the sliding mode parameters. Fig. 2 shows the given wind speed. The wind speed is set to change. When it is between 0–0.8 s, the given wind speed is 6 m/s; when it is 0.8 s, the wind speed rises to 10 m/s;

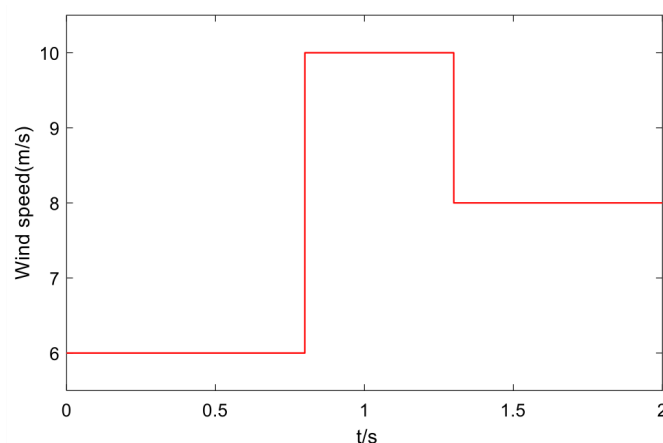


Fig. 2. Wind speed curve

finally, when 1.3 s, the wind speed drops to 8 m/s. The rotor speed is displayed in Fig. 3. It is shown that the rotor speed changes suddenly at 0.8 s and 1.3 s, and the rotor speed changes with the change of wind speed.

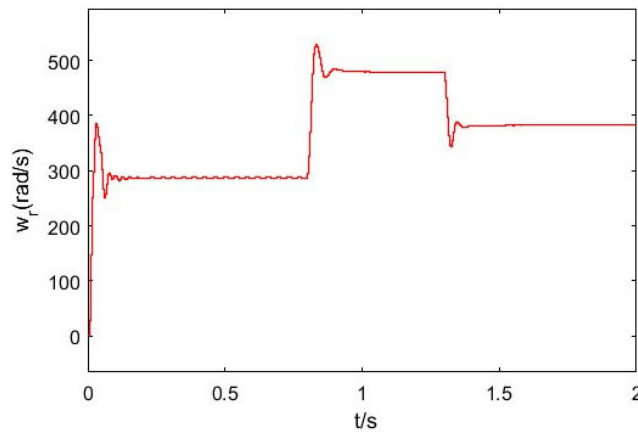


Fig. 3. Rotor speed value

Fig. 4 and Fig. 5 are the tracking curves of the measurements values and estimated values of the d -axis of the rotor current and the error curves of the d -axis measured values and estimated values of the rotor current, respectively. It can be demonstrated that there is a big error between the actual current value and the observed value at 0 s, 0.8 s and 1.3 s, but the two curves tend to coincide quickly. For example, at 0.37 s, 0.93 s and 1.5 s, the error curves are stable near 0, and their error values are 0.01944, -0.05974 and 0.01541, respectively. The q -axis case is similar to the d -axis case. Fig. 6 is the tracking curve of measurement values and estimated value of the rotor current q -axis, and Fig. 7 is the error curve of measurement values and estimated values of

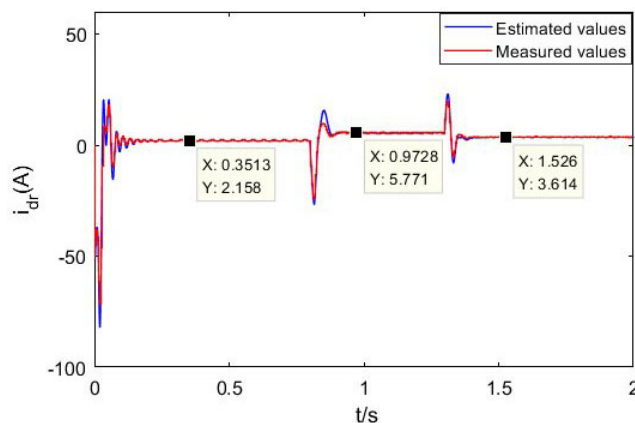


Fig. 4. Track curve of measurement value and estimated value of rotor current d -axis

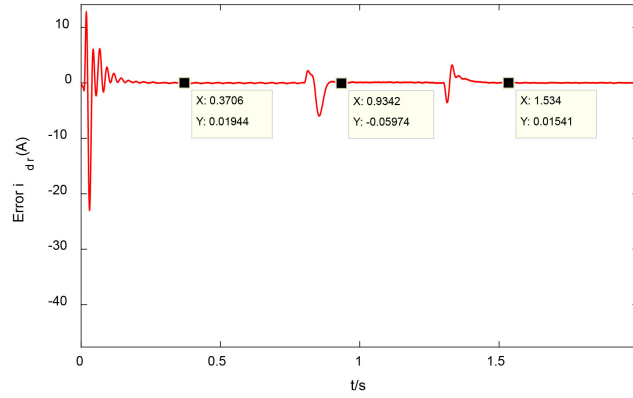


Fig. 5. Error curve of measurement value and estimated value of rotor current d -axis

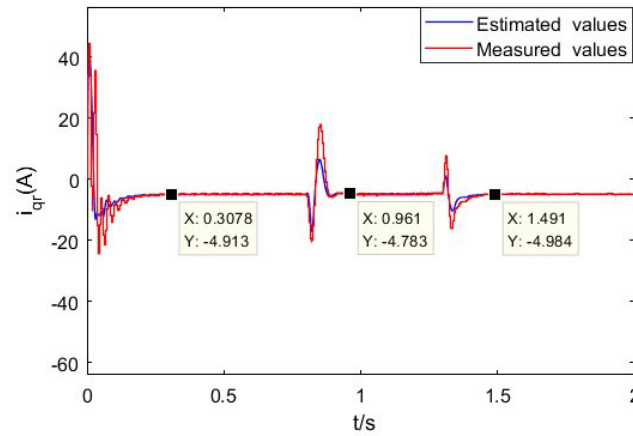


Fig. 6. Track curve of measurement values and estimated values of rotor current q -axis

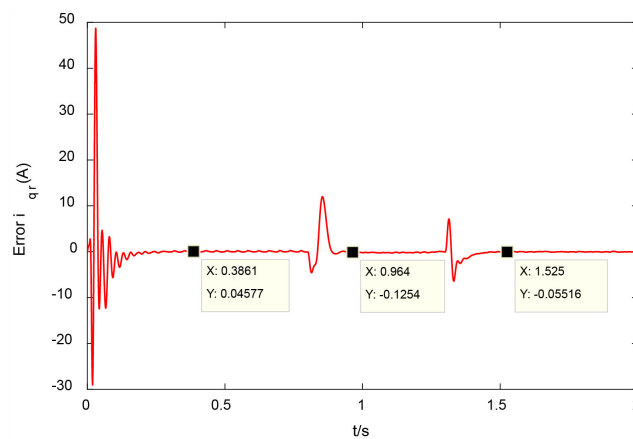


Fig. 7. Error curve of measurement values and estimated values of rotor current q -axis

the rotor current q -axis. This shows that the proposed SMO can track the rotor current very well, and have the characteristics of fast response speed and good stability.

2. Voltage drop fault

In the case of voltage sag fault on the power grid side, the voltage amplitude of the power grid input terminal is set at 311 V in this paper. The frequency value is 50 Hz, and the phase difference of three-phase ac voltage is 120° . When the fault is set at 0.6–1.4 s, the three-phase voltages A , B , and C of the grid are grounded, and then the grid voltage returns to normal after 1.4 s. $c = 2$, $g = 1$, $k = 5\,000$, $\varepsilon = 5\,000$ are set to the sliding mode parameters. Since the symmetrical three-phase voltage grounding represents the same degree of voltage amplitude drop. Equation (20) is expressed as a space vector expression in the stationary stator coordinate system.

$$u_g = U_g(1 - h)e^{j\omega_g t}, \quad (20)$$

where: U_g is the voltage amplitude of the grid, ω_g is the voltage angular velocity of the grid, and h is the percentage of the degree of failure. Fig. 8 shows the tracking curve of the measurement values and estimated values of the d -axis of the rotor current, and Fig. 9 shows the error curve of the measurement values and estimated values of the d -axis of the rotor current. When the fault is added at 0.6 s, the error curve will fluctuate greatly and quickly approach 0 or so. For example, at 0.95 s, the error is only 0.05542 A. When the fault is eliminated at 1.4 s, the jump is displayed on the d -axis error curve, and then the error curve gradually approaches zero. As can be seen from Fig. 9, the error value is -0.13 A at 1.8 s, and this value is very small. Therefore, it can be proved that the measured curve of rotor current on the d -axis can be well tracked by the estimated curve. The situation is similar for the q -axis. This paper is not going to elaborate on it. Fig. 10 shows the tracking curve of measurement values and estimated values of the q -axis of the rotor current, and Fig. 11 shows the error curve of the measurement values and estimated values of the q -axis of the rotor current.

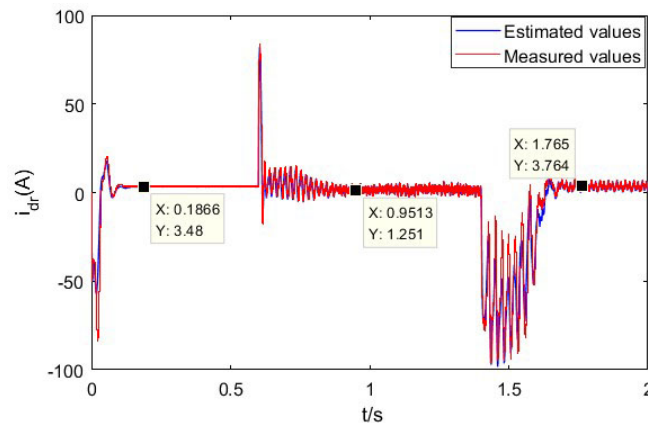


Fig. 8. Track curve of the measurement values and estimated values of the d -axis of the rotor current

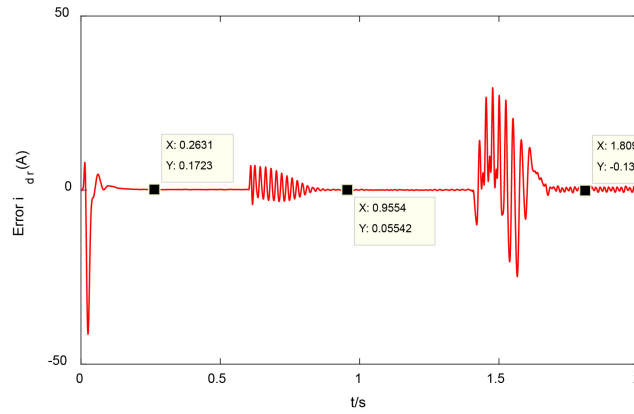


Fig. 9. Error curve of the measurement values and estimate values of the d -axis of the rotor current

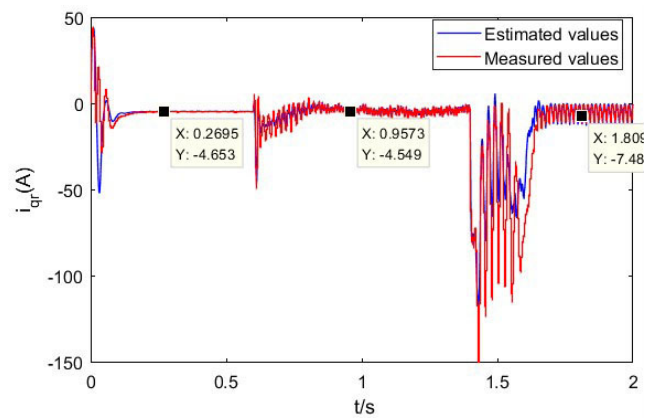


Fig. 10. Track curve of the measurement values and estimated values of the q -axis of the rotor current

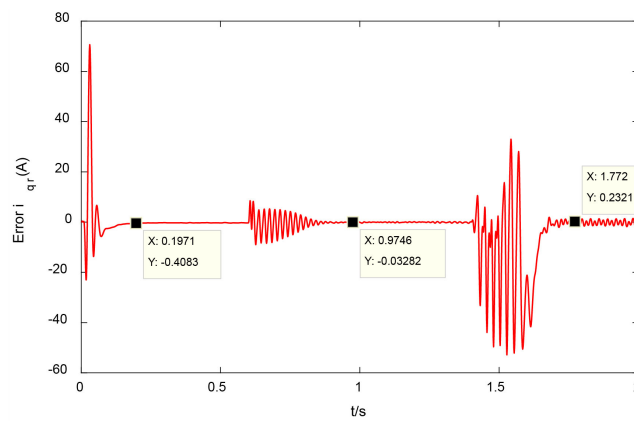


Fig. 11. Error curve of the measurement values and estimated values of the q -axis of the rotor current

3. Stator turn-to-turn fault

As the stator turn-to-turn fault is one of the main causes of induction motor failure, it is of great significance to detect it. ΔR_s is set as the change value of the stator inter-turn short circuit fault. Equation (21) is the resistance fault change value. $c = 1.312$, $g = 0.1$, $k = 5\,000$, $\varepsilon = 5\,000$ are set as sliding mode parameters in this case. Afterwards, the stator inter-turn fault can be detected by the Simulink simulation.

$$\Delta R_s = \begin{cases} 0 & 0 \leq t \leq 0.6 \\ 4 & 0.6 < t < 1.4 \\ 0 & t \geq 1.4 \end{cases} . \quad (21)$$

Fig. 12 shows the tracking curve of the measurement values and estimated values of the d -axis of the rotor current. Fig. 13 shows the error curve of the measurement values and estimated values of the d -axis of the rotor current. It can be seen from the figures that the error value is very small when no fault occurs. For example, when the error value is 0.05156 A at 0.24 s, it is approaching 0. When the fault is added at 0.6 s, the fluctuation is shown on the error curve, and then the curve error is stabilized at about 0.27 A. It can be seen from the tracking curve that the tracking effect of the measured value at the time of failure is not satisfactory. But it shows the failure. When the curve returns to normal at 1.4 s, it will jump and stabilize near zero in a very short time. It proves that the measured value can be well tracked by the estimated value. Therefore, it can be shown that the rotor current value can be well estimated through the sliding mode observer. Meanwhile, the stator inter-turn fault can be detected by the error curves of current measurements and estimates. Fig. 14 shows the tracking curve of the measurement values and estimate values of the q -axis of the rotor current. Fig. 15 shows the error curve of the q -axis measured value and estimated value of the rotor current. The q -axis current is similar to the d -axis case and will not be described.

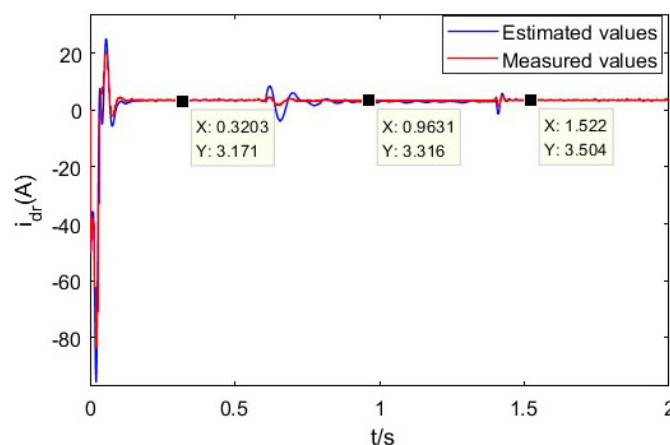


Fig. 12. Track curve of the measurement and estimated values of the d -axis of the rotor current

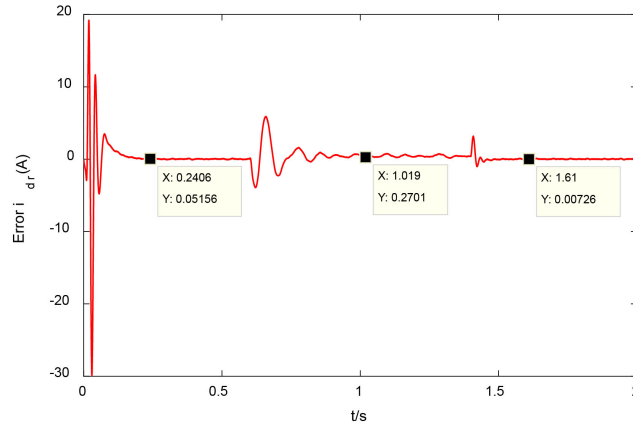


Fig. 13. Error curve of the measurement and estimated values of the d -axis of the rotor current

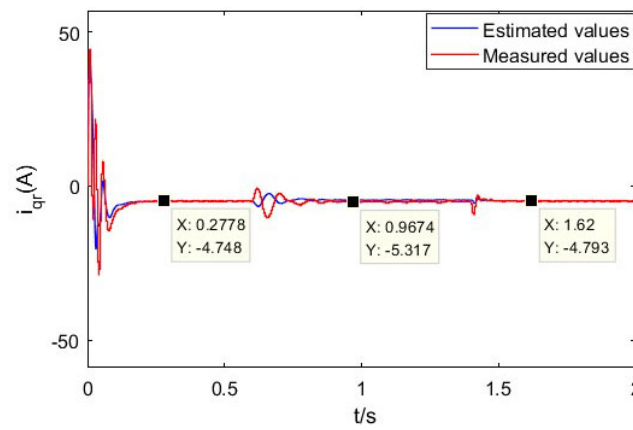


Fig. 14. Track curve of the measurement and estimated values of the q -axis of the rotor current

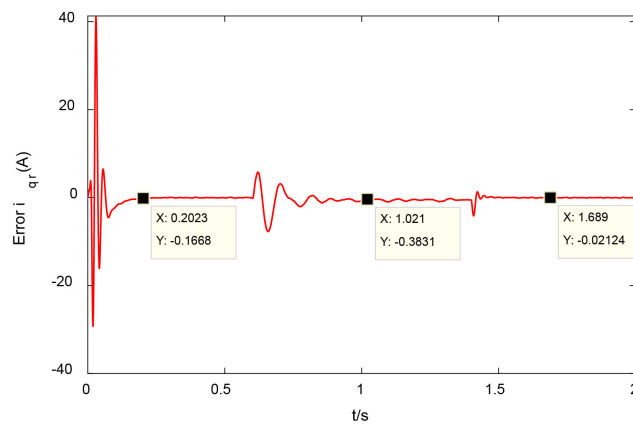


Fig. 15. Error curve of the measurement and estimated values of the q -axis of the rotor current

5. Rotor current sensor failure

When the rotor current sensor fault is considered, the fault parameters are set to $c = 1.312$, $g = 0.1$, $k = 1500$, $\varepsilon = 1500$. In this case, fault is added between 0.6 s and 1.4 s. The fault value is shown in Equation (22).

$$F = \begin{cases} 0 & 0 \leq t \leq 0.6 \\ 2e^{\cos(\pi t)} & 0.6 < t < 1.4 \\ 0 & t \geq 1.4 \end{cases} \quad (22)$$

Fig. 16 shows the tracking curve of the measurement values and estimated values of the d -axis of the rotor current. Fig. 17 shows the error curve of the measurement values and estimated values of the d -axis of the rotor current. It can be seen that the observed curve basically coincides with

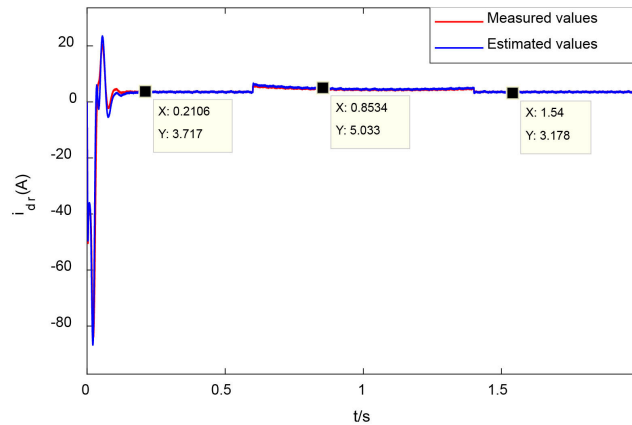


Fig. 16. Track curve of the measurement and estimated values of the d -axis of the rotor current

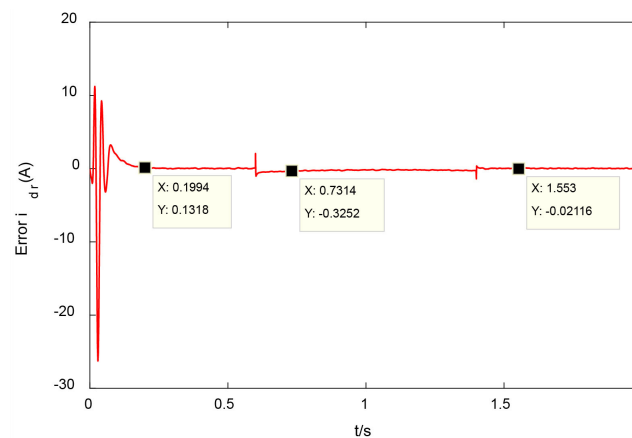


Fig. 17. Error curve of the measurement and estimated values of the d -axis of the rotor current

the actual curve. When the fault is added at 0.6 s, Fig. 17 shows that the curve fluctuates, and then the curve immediately approaches 0. When the failure is cancelled at 1.4 s, it returns to normal. The fluctuation is generated on its error curve, and the error curve is stable near 0 in an extremely short time. Thereby, the monitoring of sensor faults can be realized through the error between the actual rotor current and the observed value. Meanwhile, it can be seen from the error graph that the SMO can track the fault quickly and has good stability. Figs. 18 and 19 show the q -axis rotor current tracking curve and error curve, respectively. The q -axis curve is similar to the d -axis case.

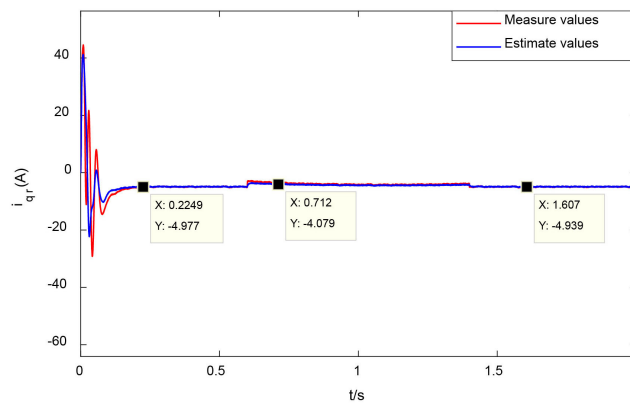


Fig. 18. Track curve of the measurement and estimated values of the q -axis of the rotor current

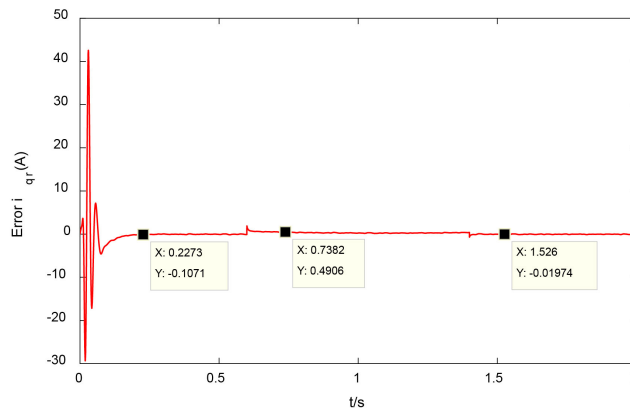


Fig. 19. Error curve of the measurement and estimated values of the q -axis of the rotor current

6. Conclusion

In this paper, a DFIG fault monitoring method is proposed using a sliding mode observer. First, a mathematical model of a DFIG is established, then a new sliding mode observer is established, and the stability and reachability of the system are analyzed. The system state is determined by

the residuals of the measured and estimated rotor currents. In this paper, four states of a fault-free state, grid terminal voltage drop fault, winding turn-to-turn short-circuit fault and current sensor fault are set. Simulations in different states are analyzed by sliding mode observers. Finally, it is verified that the sliding mode observer can perform fault monitoring on the DFIG, which has the characteristics of fast response and good stability.

Acknowledgements

This work was supported by the China Postdoctoral Science Foundation funded project No. 2017M622574.

References

- [1] Xue Z.Y., Xiahou K.S., Li M.S., Ji T.Y., Wu Q.H., *Diagnosis of Multiple Open-Circuit Switch Faults Based on Long Short-Term Memory Network for DFIG-based Wind Turbine Systems*, IEEE Journal of Emerging and Selected Topics in Power Electronics, p. 1 (2019).
- [2] Lopez J., Sanchis P., Roboam X., Marroyo L., *Dynamic Behavior of the Doubly Fed Induction Generator During Three-Phase Voltage Dips*, IEEE Transactions on Energy Conversion, vol. 22, no. 3, pp. 709–717 (2007).
- [3] Lopez J., Gubía E., Sanchis P. *et al.*, *Wind Turbines Based on Doubly Fed Induction Generator Under Asymmetrical Voltage Dips*, IEEE Transactions on Energy Conversion, vol. 23, no. 1, pp. 321–330 (2008).
- [4] Ouyang J.X., Xiong X.F., Zhang H.Y., *Characteristics of DFIG-based wind generation under grid short circuit*, Proceedings of the CSEE, vol. 31, no. 22, pp. 17–25 (2011).
- [5] Jiang S.D., Liu J., *Passive control of doubly-fed wind turbines under grid voltage drop failure*, Systems Engineering – Theory and Practice, vol. 34, no. 2, pp. 478–484 (2014).
- [6] Ma J., Liu Q., Wu J.F., Sun F.Q., Wang Y. *et al.*, *Flexible power control of rotor-side converter for doubly-fed induction generator under unbalanced voltage*, Electric Power Automation Equipment, vol. 39, no. 2, pp. 196–203 (2019).
- [7] Shah D., Nandi S., Neti P., *Stator Inter-Turn Fault Detection of Doubly-Fed Induction Generators Using Rotor Current and Search Coil Voltage Signature Analysis*, IEEE Industry Applications Annual Meeting, vol. 34, no. 2, pp. 478–484 (2014).
- [8] Ma H.Z., Zhang Z.D., Ju P. *et al.*, *Doubly-fed induction generator stator fault diagnosis based on rotor instantaneous power spectrum*, IEEE 10th International Symposium on Diagnostics for Electrical Machines, Power Electronics and Drives (SDEMPED) (2015), DOI: 10.1109/DEMPED.2015.7303685.
- [9] Mohammad Yousefi Kia, Mostafa Khedri *et al.*, *Hybrid modelling of doubly fed induction generators with inter-turn stator fault and its detection method using wavelet analysis*, IET Generation, Transmission and Distribution, vol. 9, no. 7, pp. 982–990 (2013).
- [10] Xue Z.Y., Xiahou K.S., Li M.S., Ji T.Y., Wu Q.H., *Diagnosis of Multiple Open-Circuit Switch Faults Based on Long Short-Term Memory Network for DFIG-based Wind Turbine Systems*, IEEE Journal of Emerging and Selected Topics in Power Electronics (2019), DOI: 10.1109/JESTPE.2019.2908981.
- [11] Wei Xiukun, Verhaegen M., Engelen T.V., *Sensor fault detection and isolation for wind turbines based on subspace identification and Kalman filter techniques*, International Journal of Adaptive Control and Signal Processing, vol. 24, no. 8, pp. 687–707 (2018).
- [12] Wei X., Verhaegen M., *Sensor and actuator fault diagnosis for wind turbine systems by using robust observer and filter*, Wind Energy, vol. 14, no. 4, pp. 491–516 (2011).

- [13] Ouyessaad H., Chafouk H., Lefebvre D., *Fault sensor diagnosis with Takagi–Sugeno approach design applied for DFIG wind energy systems*, International Conference on Systems and Control, IEEE (2013), DOI: 10.1109/ICoSC.2013.6750835.
- [14] Shen Y.X., Yang X.F., Zhao Z.P., *Sensor fault diagnosis for wind turbine system*, Control Theory and Applications, vol. 31, no. 3, pp. 321–328 (2017).
- [15] Wei S.R., Li Z.M., Fu Y. *et al.*, *Fault Diagnosis of Interturn Short Circuit in Stator Windings of Offshore Doubly-Fed Machines Considering the Difference of Current Estimation*, Proceedings of the CSEE, vol. 38, no. 13, pp. 3169–3977 (2018).
- [16] Lan Z.Y., Li L., Deng C., Zhang Y.Z., Yu W.X., Wong P., *A Novel Stator Current Observer for Fault Tolerant Control of Stator Current Sensor in DFIG*, 2018 IEEE Energy Conversion Congress and Exposition (ECCE) (2018), DOI: 10.1109/ECCE.2018.8557929.
- [17] Drid S., Tadjine M., Nait-Said M.S., *Robust backstepping vector control for the doubly fed induction motor*, IET Control Theory and Applications, vol. 1, no. 4, pp. 861–868 (2007).
- [18] Reigosa D.D., Guerrero J.M., Diez A.B., Briz F., *Rotor Temperature Estimation in Doubly-Fed Induction Machines Using Rotating High-Frequency Signal Injection*, IEEE Transactions on Industry Applications, vol. 53, no. 4, pp. 3652–3662 (2017).
- [19] Mojallal A., Lotfifard S., *DFIG Wind Generators Fault Diagnosis Considering Parameter and Measurement Uncertainties*, IEEE Transactions on Sustainable Energy, vol. 9, no. 4, pp. 792–804 (2018).
- [20] Abdelmalek S., Azar A.T., Dib D., *A Novel Actuator Fault-tolerant Control Strategy of DFIG-based Wind Turbines Using Takagi–Sugeno Multiple Models*, International Journal of Control Automation and Systems, pp. 1415–1424 (2018).
- [21] Li Y., Ma L., *Fault diagnosis of power transformer based on improved particle swarm optimization OS-ELM*, Archives of Electrical Engineering, vol. 68, no. 1, pp. 161–172 (2019).
- [22] Artigao E., Honrubia-Escribano A., Gomez E., *In-Service Wind Turbine DFIG Diagnosis using Current Signature Analysis*, IEEE Transactions on Industrial Electronics, vol. 67, no. 3, pp. 2262–2271 (2020).
- [23] Li W., Li Q., *Sliding mode reaching laws for suppressing chattering*, Proceeding of the 27th Chinese Control Conference, Kunming, China, pp. 154–158 (2008).